Measurement of gamma-ray production cross-sections for nuclear reactions $^{14}N(d,p\gamma)^{15}N$ and $^{28}Si(d,p\gamma)^{29}Si$

L. Csedreki[*1)], I. Uzonyi[1)], Z. Szikszai[1)], Gy. Gyürky[1)], G.Á. Szíki[2)], Á.Z. Kiss[1)]

[1)]Institute for Nuclear Research, Hungarian Academy of Sciences, MTA Atomki

H-4001 Debrecen, P.O. Box 51, Hungary

[2)]Department of Basic Technical Studies, Faculty of Engineering, University of Debrecen,

H-4028 Debrecen, Ótemető u. 2-4, Hungary

[*)] Corresponding author. Tel.: +36 52 509200; fax: +36 52 416181.

E-mail address: csedreki@atomki.mta.hu (L. Csedreki).

Abstract

In this work the differential cross sections for gamma-ray emission from the $^{14}N(d,p\gamma)^{15}N$ ($E\gamma$ = 1885, 2297, 7299 and 8310 keV) and from the $^{28}Si(d,p\gamma)^{29}Si$ ($E\gamma$ = 1273, 2028, 2426 and 4934 keV) were measured simultaneously with the $^{14}N(d,p_{4,5,6,7})^{15}N$ differential cross sections and $^{14}N(d,d)^{14}N$ elastic scattering cross section using a HPGe detector at 55^0 and an ion implanted Si detector at 135^0 with respect to the beam direction in the deuteron energy range 0.65 – 2.0 MeV. The target was a thin silicon-nitride film. Gamma-ray angular distribution measurements were performed to determine the possible anisotropy of the gamma-ray emission, and the measured cross section values were converted into total gamma-ray producing cross sections for most of the gamma-ray emissions. The average uncertainties of nitrogen and silicon gamma-ray production cross sections are 5% and 12%, respectively and 8% concerning the particle production cross section of $^{nat}N(d,d_0)^{nat}N$ and $^{14}N(d,p_{4,5,6,7})^{15}N$ reactions.

PACS: 29.30.Kv; 82.80.Ej; 81.70.-q; 25.45.-z

Keywords: DIGE; silicon-nitride film, Cross sections for gamma-ray and particles; E_d = 0.65–2 MeV;

1. Introduction

Particle induced gamma-ray emission (PIGE) is an ion beam analytical technique based on the measurement of characteristic prompt gamma-rays. It is often applied for quantitative

determination of light elemental composition of solids in their surface regions. Unfortunately, proton induced gamma-ray emission (p-PIGE) is not suitable for the determination of carbon, nitrogen and oxygen at lower incident energies due to the low gamma yields. One can overcome this disadvantage of p-PIGE by the use of deuteron induced gamma-ray emission (d-PIGE or DIGE). Since the publication of systematic measurements of absolute thick-target γ-yield curves for many elements in the region of Z = 3-20 [1], [2], several applications of the d-PIGE method have been published.

The determination of the nitrogen content of samples by d-PIGE was published in various fields of application. The first example given here is the use of d-PIGE to determine the nitrogen content of an ultra-thin silicon oxynitride film [3]. Another early work described the methodology for applying the $^{14}N(d,p\gamma)^{15}N$ nuclear reaction to measure low nitrogen levels in steel, in cases of both macro- and micro-beam analysis [4]. The applicability of the technique was also demonstrated on archaeological and ecological samples [5]. Concerning the archaeological objects, the elevated carbon and nitrogen content in the incrustations of potteries supported the hypothesis of archaeologists that the main constituent of the ornamenting white substance of certain incrusted (white decorated) potteries from the territory of Hungary could be bone grit. In the same work, a PIXE analysis of fish scale samples was completed by the measurement of lateral distributions of carbon, nitrogen and oxygen. In the work of Ager et al., nitrogen contents in micas of metamorphic rocks were measured at a nuclear microprobe [6]. Micas are minerals which provide information on geological processes due to the sensitivity of their chemical composition to temperature, pressure and deformation of rocks in which they form.

In material science, metal-organic chemical vapour deposition (MOCVD) is a wide-spread technique for the growth of thin films of large area with good composition control. Some of the recent applications of this technique concern the production of rare-earth nitride materials (like dysprosium nitride) which are of great interest for a number of applications (e.g. in spintronics) [7]. Rare-earth oxides and rare-earth-scandates are interesting for metal–oxide–semiconductor field-effect transistors (MOSFET) as well as Ge metal–oxide–semiconductor (MOS) transistors [8]. Zirconium-based thin films like zirconium oxide and zirconium nitride also have many applications (optical sensors, thermal coatings, reflectors, fuel cells as well as hard coatings, diffusion barriers, etc.) [9].The thin films obtained by MOCVD were investigated by employing a wide range of thin film analytical techniques, including X-ray diffraction (XRD), scanning electron microscopy (SEM), Rutherford backscattering (RBS) and deuteron induced gamma-ray emission (d-PIGE) analysis. D-PIGE was used either to measure the ratio of carbon, nitrogen and oxygen within the bulk of the films, or to determine the contamination level of light elements (C and N) in thin films.

In the fields of semiconductor preparation, depth profiling [10] and geological applications [6], the determination of the silicon content of materials with different kind of ion beam analytical techniques may also be required. Particle production cross sections of silicon reactions for analytical purposes were investigated extensively earlier [10,11,12], in contrast to gamma detection. Despite the lower gamma-ray production cross sections and higher detection limit, d-PIGE could be useful in some special applications, where the simultaneous

determination of light elements is required. There is even a possibility for the complex analysis of samples without standards through the combined d-PIGE/DIXE (deuteron induced X-ray emission) if the gamma-ray production cross sections are well-known. To the best knowledge of authors, gamma-ray production cross section of the $^{28}Si(d,p\gamma)^{29}Si$ reaction has not been determined in the energy range under 2 MeV yet.

This work was mainly devoted to the determination of thin target d-PIGE cross sections for the analysis of nitrogen, in the framework of a project coordinated by the International Atomic Energy Agency which aims to develop a reference database of PIGE cross-sections for ion beam analysis. As the target material was a silicon-nitride thin film, the determination of some Si gamma-ray production cross sections was also possible. In order to check the reliability of our measurement system and to get more information about the reaction mechanisms, the determination of the excitation functions of some proton groups in the $^{14}N(d,p\gamma)^{15}N$ reaction was also carried out. Gamma-ray angular distribution measurements were also performed to detect potential anisotropies which may affect the actual practice of analytical applications. The results will be uploaded to IAEA IBANDL (Ion Beam Analysis Nuclear Data Library, www-nds.iaea.org/ibandl/) to make them freely available for nitrogen and silicon determination by d-PIGE. This work is also a continuation of our earlier efforts to determine light element gamma-ray production cross sections for d-PIGE [13].

2. Experimental

The experiments were performed at the 5 MV Van de Graaff accelerator of MTA Atomki. The energy analysing device of the accelerator consists of a 90-degree homogeneous field analyzing magnet with adjustable energy defining slits before and after it. The magnetic field of the magnet is measured by a nuclear magnetic resonance (NMR) fluxmeter [14]. The calibration constant giving the relation between the particle energy and NMR frequency [15] was determined independently using the resonance of the $^{27}Al(p,\gamma)^{28}Si$ reaction at 991.86 ± 0.03 keV [16] and the $^{7}Li(p,n)^{7}Be$ reaction threshold at 1880.44±0.02 keV [17]. Target materials applied for these measurements were a 750 nm thick Al foil, and a 135 μg/cm^2 thick LiF evaporated on Ta backing, respectively. The calibration around 992 keV was repeated several times (before and after the cross section measurement with deuteron beams) at the same slit settings and new calibration constants were calculated. As a result, the obtained calibration constants varied within 0.3 %, which means that the uncertainty in the proton beam energy of the accelerator was of the order 3 keV in the 900 –1900 keV energy range. According to the formula given for the calibration constant in ref. [15], we can suppose that this value is also valid for a deuteron beam.

The deuteron beam after passing through a switching magnet was transported to a PIGE reaction chamber modified to this project and installed to the J30 beam-line. The rather small chamber (with a diameter of 9.5 cm) was insulated from the rest of the beam pipe, and had several diaphragms in its long entrance tube to form a beam of 1 mm diameter and also to

eliminate secondary particles, and ended in a long Faraday cup. The analysed deuteron beam did not exceed 100 nA, while the beam current measured in the chamber was kept between 20 and 50 nA during the measurements. The accumulated beam charge was measured by an ORTEC 439 Digital Current Integrator and varied between 20 and 400 μC for each single run depending on the deuteron energy. In order to determine the stochastic uncertainty of the current integration, yield determination was made using an Al foil of 750 nm thickness. Based on the yield measurements for the 1779 keV aluminium peak in the $^{27}Al(p,\gamma)^{28}Si$ reaction, the stability of charge integration was better than 1%.

Gamma-rays were detected with a CANBERRA Model GR4025-7600SL coaxial type HPGe detector (diameter: 59.5 mm, volume of the crystal: 170 cm^3, energy resolution: 2.3 keV at 1.33 MeV) installed on one of the two arms of a turntable at an angle of θ=55° relative to the incident beam direction. The front face of the detector was 9.5 cm and 20.7 cm far from the target in case of excitation function and angular distribution measurements, respectively. The detector was surrounded by a lead shield of 5 cm thickness, and additional shields built from lead bricks were applied close to the entrance diaphragms as well as the Faraday cup to protect the detector against gamma-rays originated from them. The inner wall of the target chamber was covered with a copper lining to decrease gamma radiation caused by backscattered particles in the stainless steel wall of the chamber. The gamma-ray background in our experimental arrangement was determined with a deuteron beam let through the chamber. It turned out to be less than 2.5% in all the studied peaks which was taken into account in the cross section calculations.

The target chamber had an inlet for a particle detector at $\beta=135^o$ relative to the beam axis. An ORTEC ion-implanted silicon detector with 500 μm active depth and 35 keV energy resolution was installed in it. A 3 mm diameter copper collimator in front of the detector served to reduce high intensity backscattered particles and to define a solid angle for the detector. The determination of the solid angle of the Si detector was done with alpha-RBS and a Th(B+C) radioactive source with a well known activity. Based on these methods, the solid angle was found to be 5.8 ± 0.1 msr. This set-up was intended to detect the backscattered particles from the target. The novelty of this experimental arrangement compared to our previous one [13] is the simultaneous measuring of gamma-rays and particles from the reactions investigated, which gives the possibility of continuous target thickness determination when the elastic backscattering cross section is considered as Rutherford, and which contributes to the reliable determination of the excitation functions, in this case belonging to the $^{14}N(d,p_{4,5,6,7})^{15}N$ reactions. The schematic drawing of the chamber and the experimental set-up is shown in Fig. 1.

Determination of the efficiency of the gamma-ray detector

In order to determine the absolute efficiency (ε_{abs}) of the gamma-ray detector for every nitrogen and silicon gamma-line, radioactive sources supplemented with narrow resonance reactions were used. For the E_γ < 3500 keV region, radioactive sources such as ^{133}Ba, ^{56}Co,

^{60}Co, ^{137}Cs and ^{152}Eu were placed at the exact position of the target. The sources (except ^{56}Co) were calibrated previously by the Hungarian National Office of Measures. For the E_γ > 3500 keV region, the detector efficiency was determined using gamma-cascades from the ^{23}Na(p,γ)^{24}Mg and ^{27}Al(p,γ)^{28}Si reactions at 1417 and 992 keV resonance energies, respectively. An approx. 100nm thick Na_2WO_4 layer evaporated onto a self-supported carbon foil and a 750nm thick aluminium foil served as targets. The applied relative intensities of the reactions are taken from refs. [18] and [19]. In order to determine the absolute full-energy peak efficiency curve fitted on the calibration points, two different formulas were applied in the case of photo peaks, one for energies below 3.5 MeV, and another one from 2 MeV up to 10 MeV. The first formula was calculated with a power-function recommended by Abriola et al. [20] and the second one was a third-order polynomial. The absolute double escape efficiency was calculated using a fourth-order polynomial. With this, the contribution of the double escape line of the 8310 keV gamma-line could be separated from the 7299 keV gamma-line in the gamma-ray production cross section calculations.

Description of the experimental set-up, energy calibration of the accelerator, particle detector solid angle determination and the procedure of the absolute efficiency determination of the gamma-ray detector is also published in [21].

Target properties

A thin film of Si_xN_y (x=1, y=1±0.05, thickness: 200±14 nm, area: 5×5mm^2, data was provided by the manufacturer, Norcada Inc.) was selected as a target in order to measure cross-section as a function of energy. During the measurements, gamma-rays, protons and backscattered deuterons were detected simultaneously. Below 0.95 MeV the backscattering of deuterons on nitrogen can be considered as Rutherford [22]. The respective value for silicon is 1.6 MeV. Below these energies we could determine the number of target atoms (N_t) at each energy point E_0 with equation (1).

$$N_t = \frac{Y(E_0,\beta)}{\frac{d\sigma_{Ruth}(E_0,\beta)}{d\Omega} N_p \Omega \varepsilon}, \quad (1)$$

In the above equation $Y(E_0,\beta)$ is the scattered projectile yield for the given element in the target (i.e. the area of the scattered projectile peak corrected for live time) measured at projectile energy E_0 and particle detection angle β, $d\sigma_{Ruth}(E_0,\beta)/d\Omega$ is the Rutherford cross section for the given element at projectile energy E_0 and particle detection angle β, ε is the intrinsic efficiency of the particle detector (~100%), Ω is the solid angle of particle detection (assumed to be small), N_p is the number of incident projectiles which can be calculated as the ratio of the accumulated (Q) and elementary (e) charge.

Averaging the N_t values measured at various energies (nitrogen: 0.65-0.95 MeV, silicon: 0.65-1.60 MeV), we obtained (7.80±0.20)*10^{17} and (6.95±0.10)*10^{17} atom/cm^2 for nitrogen and silicon, respectively. In order to check these data we also performed measurements with alpha-RBS technique at incident energy of 1.5 MeV under the same experimental conditions. In this case the respective values were (7.73±0.20)*10^{17} and (7.02±0.10)*10^{17} atom/cm^2. The system accuracy was checked using palladium evaporated onto silicon backings with well

defined thicknesses, as standards. Based on RBS-methods, and considering the uncertainties, we accepted the $(7.77\pm0.20)*10^{17}$ and $(6.99\pm0.10)*10^{17}$ atom/cm^2 values for nitrogen and silicon, respectively.

In the case of nitrogen and silicon, the different isotopes are not separated in the RBS spectra. Thus the number of ^{14}N and ^{28}Si nuclides in the target was calculated from the above data taking into account the 0.9963 and 0.9223 natural isotopic ratios of ^{14}N and ^{28}Si.

Gamma-ray and particle yield measurements

As both nitrogen and silicon have rather complicated d-PIGE spectra (see figs. 4. and 10. in ref. [2]), in the case of silicon nitride even more complicated spectra were expected. Only relatively intense gamma-rays which could also be separated from others were selected for yield measurements. In the case of nitrogen these were: 1885 keV [^{14}N(d,p$\gamma_{4\text{-}1}$)^{15}N], 2297 keV [^{14}N(d,p$\gamma_{6\text{-}1}$)^{15}N], 7299 keV [^{14}N(d,p$\gamma_{5\text{-}0}$)^{15}N] and 8310 keV [^{14}N(d,p$\gamma_{7\text{-}0}$)^{15}N], where the subscript shows the numbers of the two states between which the transition occurs. The 7299 keV energy ^{14}N(d,p$\gamma_{5\text{-}0}$)^{15}N gamma-ray is the strongest one, however its full energy (FE) peak is contaminated by the double escape (DE) peak of the 8310 keV gamma-ray. For the determination of the cross section of this gamma-ray we had to subtract the above mentioned DE peak, based on the known absolute FE and DE efficiency curves of the HPGe detector. For silicon 1273keV [^{28}Si(d,p$\gamma_{1\text{-}0}$)^{29}Si] , 2028 keV [^{28}Si(d,p$\gamma_{2\text{-}0}$)^{29}Si], 2426 [^{28}Si(d,p$\gamma_{3\text{-}0}$)^{29}Si] and 4934 keV [^{28}Si(d,p$\gamma_{10\text{-}0}$)^{29}Si] gamma-ray yields were measured. Although the applied particle detector had a rather poor energy resolution, and the electronic set-up was optimized to detect the backscattered Si peak, it was still possible to measure the yields of the ^{14}N(d,p$_4$)^{15}N, ^{14}N(d,p$_5$)^{15}N, ^{14}N(d,p$_6$)^{15}N, and ^{14}N(d,p$_7$)^{15}N reactions and the ^{14}N(d,d$_o$)^{14}N elastic scattering simultaneously with the gamma-ray yields. Fig.2. shows a typical particle spectrum, measured at 135^0 with 2 MeV deuteron beam. The cross section measurements were carried out with 50 keV steps from 2 MeV to 0.65 MeV, and at certain points the measurement was repeated in two additional runs.

3. Determination of cross sections and discussion of the results

3.1 Gamma-ray production cross sections

Differential cross sections were calculated according to the following equation [23]:

$$\frac{d\sigma(E_0,\theta)}{d\Omega} = \frac{Y_\gamma(E_0,\theta)}{N_p N_T \varepsilon_{abs}(E_\gamma) 4\pi} \quad (2)$$

where $Y_\gamma(E_0,\theta)$ is the measured γ-ray yield (i.e. the net area of the γ-ray peak corrected for live time) at projectile energy E_0 and γ-ray detection angle θ, N_p is the number of incident projectiles, N_T is the number of target nuclei per square centimeter and $\varepsilon_{abs}(E_\gamma)$ is the absolute efficiency of the HPGe detector corresponding to the E_γ energy γ-ray line.

Concerning the measured gamma-ray yields (Y_γ), the uncertainties were below 4% in the case of every nitrogen transition and varied between 1-40% for the silicon gamma-lines which depended strongly on the incident deuteron energy and the silicon reaction channel.

After the accurate determination of the experimental parameters, we considered the possible uncertainties in the following way. The error of N_t was 2.5% based on alpha and deuteron-RBS measurements. The stochastic and systematic uncertainty of charge determination was taken into account with 3%. For the absolute efficiency (ε_{abs}) 2% was assigned from fitting the experimental data. The errors were added quadratically and these values are indicated in the cross section figures. The average uncertainties of the nitrogen and silicon gamma-ray production cross sections are 5% and 12%.

Gamma-ray angular distributions

From *Equation (2)* the total gamma-ray production cross section can be calculated by a multiplication with 4π only in the case if the gamma-ray angular distribution is definitely isotropic, which is guaranteed e.g. if the initial state of the transition has a ½ spin value [24] The spin-parity values of initial states of the studied gamma transitions are summarized in Table 1. Owing to the spin of the initial state, only the angular distribution of the 8310 keV gamma-rays must be isotropic. For all other gamma-rays one has to determine the anisotropy experimentally. This experiment was performed using a deuteron beam of 1.95 MeV at laboratory angles of 30°, 45°, 55°, 75°, 90°, 120°, and 135°.

In both reactions the measured gamma yields Y_γ as a function of detection angle were fitted with a Legendre polynomial expansion using the following formula:

$$Y_\gamma = A_0 \times (1 + A_2 P_2(cos\theta)) \quad (3)$$

where A_0 and A_2 are the fit parameters, θ is the angle in the c.m. frame and higher order terms of the expansion are neglected. The best fit values and uncertainties of the A_2 parameter, which reflects the (an)isotropy of the transition are listed in Table 1. For the 8310 keV gamma transition the A_2 parameter is consistent with zero within two sigma statistical uncertainty. This fit is shown in fig. 3A. where the thick line shows the best fit curve while the thin contours represent the one sigma uncertainty band. In the case of a few transitions significant anisotropy is observed. An example is shown in fig. 3B. where the angular distribution of $^{28}Si(d,p\gamma_{3\text{-}0})^{29}Si$ reaction channel, having the highest A_2 value is shown.

The total cross sections of the present work (see below) were obtained by multiplying the differential cross section measured at 55° by 4π. Owing to the observed anisotropy in the case of a few studied transitions, variation of up to 23% can be expected if measurements are carried out at different detection angles. Therefore, for analytical purposes we recommend to carry our gamma detection at 55° where the effect of the angular distribution is the smallest.

As a result of the present experiments, Fig 4 shows the total gamma-ray production cross sections and the corresponding errors of $^{14}N(d,p\gamma)^{15}N$ reactions as a function of bombarding energy. For comparison, the data of Bebber et al. [3], the only data found in literature for nitrogen is presented. The total/differential gamma-ray production cross sections of

$^{28}Si(d,p\gamma)^{29}Si$ reactions determined in this work are presented in Fig 5. For this reaction, no previous data have been found in the literature.

Considering the $^{14}N(d,p\gamma)^{15}N$ reactions in fig. 4., the energy dependence of the obtained cross sections show deviations from the direct reaction mechanism. This is clearly seen in the case of the 1885 keV $^{14}N(d,p\gamma_{4\text{-}1})^{15}N$ gamma-ray, where a pronounced maximum is seen in the cross section function in the studied energy interval. Bebber et al. only measured the total cross sections of the 7299 keV energy $^{14}N(d,p\gamma_{5\text{-}0})^{15}N$ and 8310 keV $^{14}N(d,p\gamma_{7\text{-}0})^{15}N$ gamma-rays over the deuteron energy range of 500-1500 keV. However, they used a 4π gamma detector avoiding the problem of escape peaks disturbing other gamma peaks, and they obtained total cross sections independently from angular distributions. The discrepancy between the present and Bebber's results are not fully understood.

The energy dependence of the $^{28}Si(d,p\gamma)^{29}Si$ cross sections reflect much more the direct reaction mechanism, with two exception. Firstly is the local maximum in the excitation function of $^{28}Si(d,p\gamma_{2\text{-}0})^{29}Si$ and $^{28}Si(d,p\gamma_{3\text{-}0})^{29}Si$ reaction at 1950 keV deuteron energy and another is at 1350 keV deuteron energy, where a local maximum emerges from the monotonously increasing yield in all four cases. One has to note that the error bars are quite large due to the smaller counting statistics.

3.2 **Particle production cross sections**

Particle production cross sections from the simultaneously measured particle yields were also determined and compared with literature data to corroborate the validity of our gamma-ray production cross sections.

The particle production cross section can be written as:

$$\frac{d\sigma(E_0,\beta)}{d\Omega} = \frac{Y(E_0,\beta)}{N_p N_t \Omega \varepsilon} \qquad (4)$$

where $d\sigma(E_0,\beta)/d\Omega$ is the differential particle production cross section at deuteron energy E_0 and particle detection angle β , $Y(E_0,\beta)$ is the measured particle yield (i.e. the net area of the particle peak corrected for live time) measured at deuteron energy E_0 and particle detection angle β, ε is the intrinsic efficiency of the particle detector (usually ~100%), Ω is the solid angle of particle detection (assumed to be small), N_p is the number of incident ions and N_t is the number of target nuclei per square centimeter. Uncertainties of the measured particle yields of nitrogen varied between 1-7%. The precision of the solid-angle determination of the particle detector (Ω) was 2.5%, which also includes the radioactivity determination of the Th(B+C) source. The average uncertainty concerning the particle production cross sections of $^{nat}N(d,d_0)^{nat}N$, $^{14}N(d,p_{4,5,6,7})^{15}N$ reactions is estimated as 8%.

The differential cross sections of the $^{14}N(d,p_{4,5,6,7})^{15}N$ reactions and the $^{14}N(d,d_o)^{14}N$ elastic scattering at laboratory angle of 135^0 were determined with this method. The present results compared with the literature data obtained also at 135^0 are shown in fig. 6. and fig. 7. for the (d,p) reactions and the (d,d) elastic scattering, respectively. All parameters are given in laboratory system. The p_4, p_6 and p_7 differential cross sections show pronounced maxima in the studied deuteron energy region, which indicates the mixture of compound and direct reaction mechanisms.

Contrary to the reaction $^{14}N(d,p\gamma)^{15}N$, several work were published for $^{14}N(d,p)^{15}N$ below E_d = 5 MeV till the eighties [26-32] and two works recently [33,34]. Previous results were compiled in [35- 37]. Because of the high Q value of the reaction, very high states are excited in the compound nucleus ^{16}O ($E_x \geq 20$ MeV). According to the compilation of Ajzenberg-Selove [35], the excitation functions of the proton groups do not show resonances below E_d<5 MeV but merely fluctuations. These are at E_d = 1.4, 1.7, 1.85 and 2.0 MeV in the energy range studied by us. The most detailed work was done by V. Gomes Porto et al. [26]. They measured the differential cross section of several proton groups and their angular distributions in the energy range $1.0 \leq \boldsymbol{E_d} \leq 3.1$ MeV. They analysed these data using the optical model and the Hauser-Feshbach and DWBA theories, and concluded that both direct interaction and compound nuclear processes must be considered, based on the systematic trend as a function of energy and the fluctuations about the average behaviour. A broad resonance around 2 MeV was also found in the excitation function of $^{14}N(d, p_5)^{15}N$ reaction which were attributed to a kind of intermediate structure.

For the $^{14}N(d,p_{4,5,6,7})^{15}N$ reactions, only the differential cross sections of Valek et al [30] and Beaumevielle et al.[28] were measured at ~135^0 and can be compared directly with our results. Moreover Valek et al. measured below 0.638 MeV while Beaumevielle had only a few measured points (see fig.6). These are rather limited data; nevertheless, they are close to our values, showing the same energy dependence. Thus our values can be considered as new contribution concerning the $^{14}N(d,p)^{15}N$ reactions. The fluctuations in the case of p4, p5 and p6 groups support the statement of Ajzenberg-Selove [36] about the resonant structure. Our (d,pγ) results, especially the excitation function of the 4-1 gamma transition, also shows the resonant structure around 1.4 MeV deuteron energy. Qualitatively similar energy dependence with a maximum is shown for the p4, p6 and p7 differential cross sections measured at different c.m. angles (118.3^0, 150^0 167.1^0, etc.) by other authors [26, 31, 33].

Considering the elastic scattering, no previous data are found at the same angle. Only Seiler et al. have measurements close to 135^0 at 125.3 and 140.8 degrees [38]. The deviation from the Rutherford character is clearly seen.

4. Summary

The main aim of the present work was to determine the total gamma-ray production cross section of $^{14}N(d,p\gamma_{4-1})^{15}N$, $^{14}N(d,p\gamma_{6-1})^{15}N$, $^{14}N(d,p\gamma_{5-0})^{15}N$, $^{14}N(d,p\gamma_{7-0})^{15}N$,$^{28}Si(d,p\gamma_{1-0})^{29}Si$, $^{28}Si(d,p\gamma_{2-0})^{29}Si$, $^{28}Si(d,p\gamma_{3-0})^{29}Si$, $^{28}Si(d,p\gamma_{10-0})^{29}Si$ reactions. Secondly, we investigated the gamma-ray angular distribution of these reactions, which were considerably close to isotropic; these deviations can influence only slightly the measurements in IBA practice. In addition, the pronounced maximum in the cross section function of the 1885 keV $^{14}N(d,p\gamma_{4-1})^{15}N$ gamma-ray, found around 1.4 MeV deuteron energy, called our attention to the particle spectra measured simultaneously with the gamma spectra. Although the original idea was to use only the elastic scattered peaks from these particle spectra to determine the number of projectiles and target atoms, we could also detect the $^{14}N(d,p_4)^{15}N$, $^{14}N(d,p_5)^{15}N$, $^{14}N(d,p_6)^{15}N$, and $^{14}N(d,p_7)^{15}N$ proton groups, widening the original scope of our work. The gamma-ray and particle cross section data will be soon available to the ion beam community through IBANDL (Ion Beam Analysis Nuclear Data Library), hopefully opening up new possibilities for applications of the d-PIGE method.

Acknowledgement

The support of the IAEA Coordinated Research Project “Reference Database for Particle-Induced Gamma-ray Emission (PIGE) Spectroscopy” (Contract No. 16967/R1) is acknowledged.

References

[1] Á. Z. Kiss, I. Biron, T.Calligaro, J. Salomon, Nuclear Instruments and Methods in Physics Research B 85 (1994)118-122.

[2] Z. Elekes, Á.Z. Kiss, I. Biron, T. Calligaro, J. Salomon, Nuclear Instruments and Methods in Physics Research B 168 (2000) 305-320

[3] H. van Bebber, L. Borucki, K. Farzin, Á.Z. Kiss, W.H. Schulte, Nuclear Instruments and Methods in Physics Research B 136138 (1998) 72-76. (data retrieved from the IBANDL database, http://www-nds.iaea.org/ibandl/).

[4]F.J. Ager, S. Elmrabet, A. Paúl, Á. Cea-Naharro, M. D. Ynsa, M. A. Respaldiza, J. A. Odriozola, Nuclear Instruments and Methods in Physics Research B: 188 (2002) 96-101.

[5] G. Á. Szíki, I. Uzonyi, E. Dobos, I. Rajta, K. T. Biró, S. Nagy, Á. Z. Kiss, Nuclear Instruments and Methods in Physics Research B 219–220 (2004) 508–513.

[6] F.J. Ager, M.P. Mata, M.D. Ynsa, M.A. Respaldiza, B. Goffe, F. Nieto, Nuclear Instruments and Methods in Physics Research B 249 (2006) 642–645.

[7] T. B. Thiede, M. Krasnopolski, A. P. Milanov, T. de los Arcos, A. Ney, H-W. Becker, D. Rogalla, J. Winter, A. Devi, and R. A. Fischer, Chemistry of Materials, 23 (2011) 1430–1440.

[8] A. P. Milanov, Ke Xu, S. Cwik, H. Parala, T. de los Arcos, H-W. Becker, D. Rogalla, R. Cross, S. Pauld and A. Devi, Dalton Trans. 2012.

[9] M. Banerjee, N. B. Srinivasan, H. Zhu, S. Ja Kim, Ke Xu, M. Winter, H-W. Becker, D. Rogalla, T. de los Arcos, D. Bekermann, D. Barreca, R. A. Fischer, and A. Devi, Crystal Growth Design, 12 (2012) 5079−5089.

[10] A.F. Gurbich and S.L. Molodtsov, Nuclear Instruments and Methods in Physics Research B 226 (2004) 637-643.

[11] M. Kokkoris, K. Michalakis, P. Misaelides, A. Lagoyannis, S. Harissopulos, R. Vlastou, C.T. Papadopoulos, Nuclear Instruments and Methods in Physics Research B 267 (2009) 1744.

[12] S. Pellegrino, L. Beck, Ph. Trouslard, P. Trocellier, Nuclear Instruments and Methods in Physics Research B 266 (2008) 2268-2272.

[13] G.Á. Sziki, A. Simon, Z. Szikszai, Zs. Kertész, E. Dobos, Nuclear Instruments and Methods in Physics Research B 251 (2006) 343-351.

[14] Á.Z. Kiss, E. Koltay, Gy. Mórik, A. Paál, M. Rubecz, E. Somorjai, Atomki Közlemények 20 (1978) 89-111.

[15] J. B. Marion, F.C. Young, Nuclear Reaction Analysis. Graphs and Tables. North Holland Publishing Co. Amsterdam, 1968.

[16] P. M. Endt, Nuclear Physics A521 (1991) 1.

[17] F. Ajzenberg-Selove, Nuclear Physics A490 (1988) 1.

[18] Z. Elekes, T. Belgya, G. L. Molnár, Á. Z. Kiss, M. Csatlós, J. Gulyás, A. Krasznahorkay, Z. Máté, Nuclear Instruments and Methods in Physics Research A 503 (2003) 580-588.

[19] A. Anttila, J. Keinonen, M. Hautala and I. Forsblom, Nuclear Instruments and Methods 147 (1977) 501-505

[20] D. Abriola and A. Pedro de Jesus, Summary Report 1st Research Coordination Meeting Development of a Reference Database for Particle-Induced Gamma-ray Emission (PIGE) Spectroscopy, IAEA Headquarters, Vienna, Austria, 16-20 May 2011, INDC (NDS)-0589.

[21] L. Csedreki, Acta Physica Debrecina **46** (2012) 25-35.

[22] M. Bozoian, Nuclear Instruments and Methods in Physics Research B 58 (1991) 127.

[23] D. Abriola, P. Dimitriou and A. Pedro de Jesus, Summary Report 2nd Research Coordination Meeting Development of a Reference Database for Particle-Induced Gamma-ray Emission (PIGE) Spectroscopy, IAEA Headquarters, Vienna, Austria, 8-12 October 2012, INDC(NDS)-0625.

[24] S. Devons, L. J. B. Goldfarb, Angular Correlations, Nuclear Reactions III., Series: Encyclopedia of Physics, Springer Berlin Heidelberg (Berlin, Heidelberg), vol. 8 / 42, pp. 362-554.

[25] F. Ajzenberg-Selove, Nuclear Physics A523 (1991) 1.

[26] V. Gomes Porto, N. Ueta, R. A. Douglas and O. Sala, D. Wilmore, B. A. Robson, P. E. Hodgson, Nuclear Physics A136 (1969) 385-413.

[27] G. Amsel et D. David, Rev. Phys. Appl. (Paris) 4, (1969) 383-391.

[28] H. Beaumevieille, M. Lambert, M. Yaker and A. Amokrane, Nuclear Physics A125 (1969) 568-584. (data retrieved from the IBANDL database, http://www-nds.iaea.org/ibandl/).

[29] A. V. Nero, R. E. Pixley and E. G. Adelberger, Physical Review C 6 (1972) 679.

[30] A. Valek, T. Vertse, B. Schlenk and I. Hunyadi, Nuclear Physics A270 (1976) 200- 210. (data retrieved from the IBANDL database, http://www-nds.iaea.org/ibandl/).

[31] W. Koenig, A. Riccato, R. Stock, P. Cuzzocrea, E. Perillo, M. Sandoli, G. Spadaccini, Nuovo Cimento A39 (1977) 9.

[32] A. Niiler and R. Birkmire, Nuclear Instruments and Methods 168 (1980) 105-109;

[33] S. Pellegrino, L. Beck, Ph. Trouslard, Nuclear Instruments and Methods in Physics Research B 219–220 (2004) 140–144.

[34]A. Gurbich, . Bogdanović-Radović, M. Chiari, C. Jeynes, M. Kokkoris, A.R. Ramos, M. Mayer, E. Rauhala, O. Schwerer, Shi Liqun, I. Vickridge, Nuclear Instruments and Methods in Physics Research B 266 (2008) 1198–1202

[35] F. Ajzenberg-Selove, Nuclear Physics A375 (1982) 1.

[36] F. Ajzenberg-Selove, Nuclear Physics A281 (1977) 1.

[37] F. Ajzenberg-Selove, Nuclear Physics A166 (1971) 1.

[38] R.F.Seiler, D.F.Herring, K.W.Jones, Phys. Rev. 136 (1964) 994. (data retrieved from the IBANDL database, http://www-nds.iaea.org/ibandl/).

Figure capture:

Fig. 1. Schematic view of the experimental setup. 1: beam, 2: current measuring points, 3: collimators, 4: target, 5: Si particle detector, 6: HPGe detector, 7: lead shields

Fig. 2. Typical particle spectrum, measured at 135^0 with 2 MeV deuteron beam. (The carbon peaks are due to a slight carbon build up on the target.)

Table 1. Summary of the properties and angular dependence of nitrogen and silicon reactions, $A_2 \pm \Delta A_2$: fit parameters and their errors, see eq. 3. [16, 25]

Fig. 3A, 3B. Summary of the results of the gamma-ray angular distribution measurements. Thick line shows the best fit curve while the thin contours represent the one sigma uncertainty band.

Fig.4. Excitation function of differential N+d reactions

Fig.5. Excitation function of differential Si+d reactions

Fig. 6. and 7. Particle production cross sections of $^{14}N(d,_{p4,5,6,7})^{15}N$ and $^{nat}N(d,d_0)^{nat}N$ reactions. Ref [30] was made with magnification 800.

Figures

Fig.1

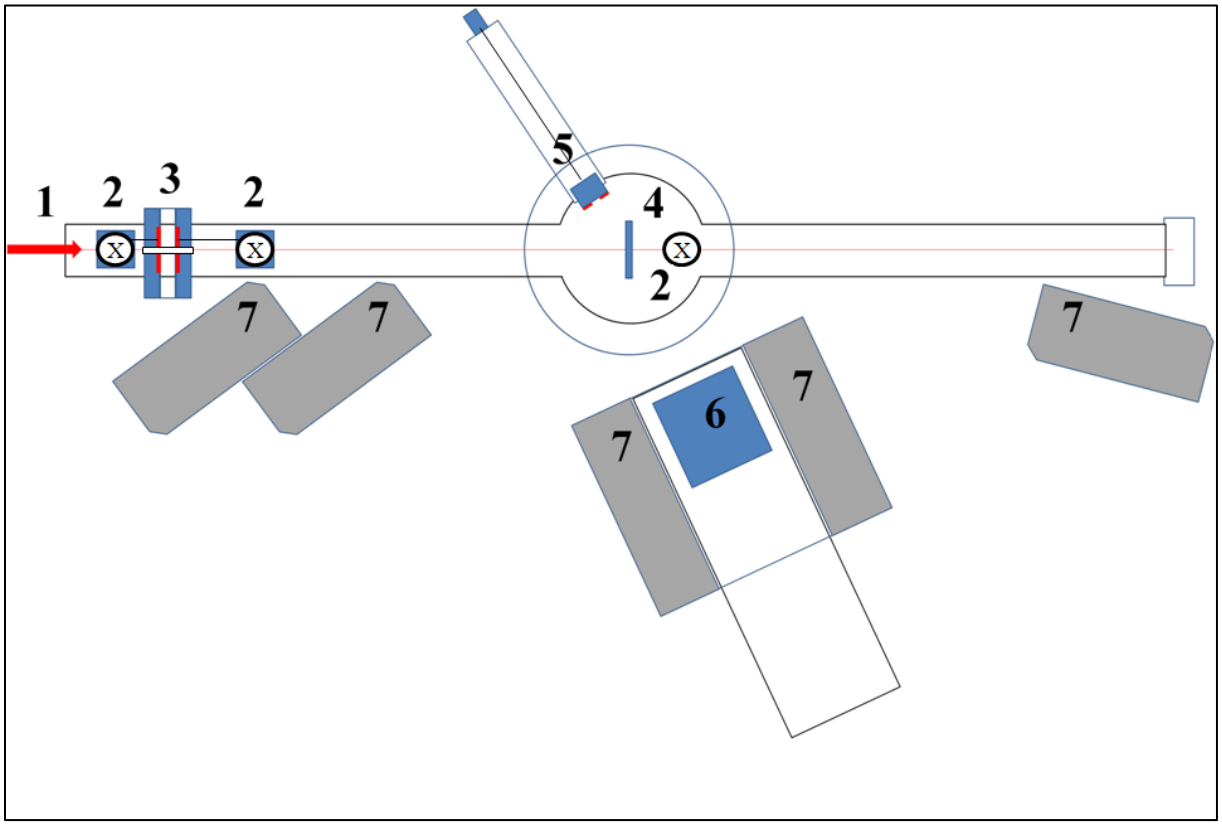

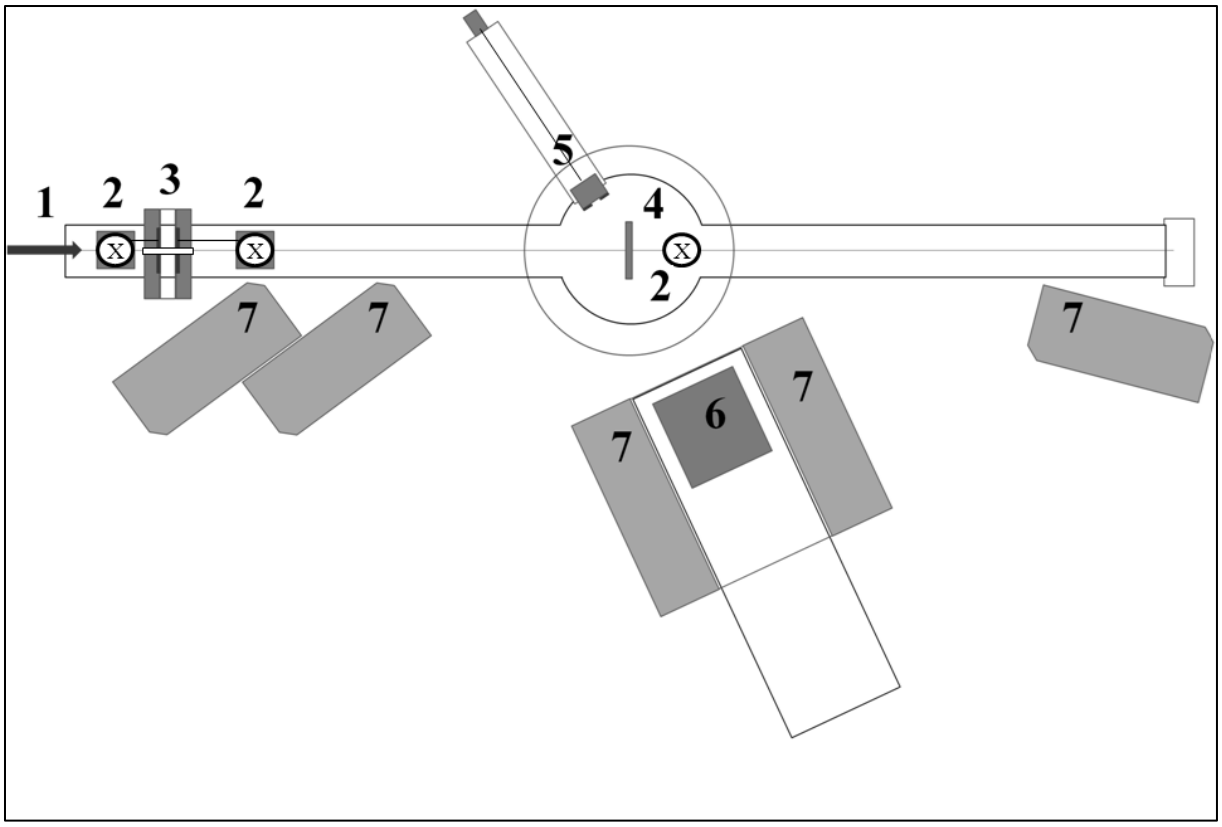

Fig. 2

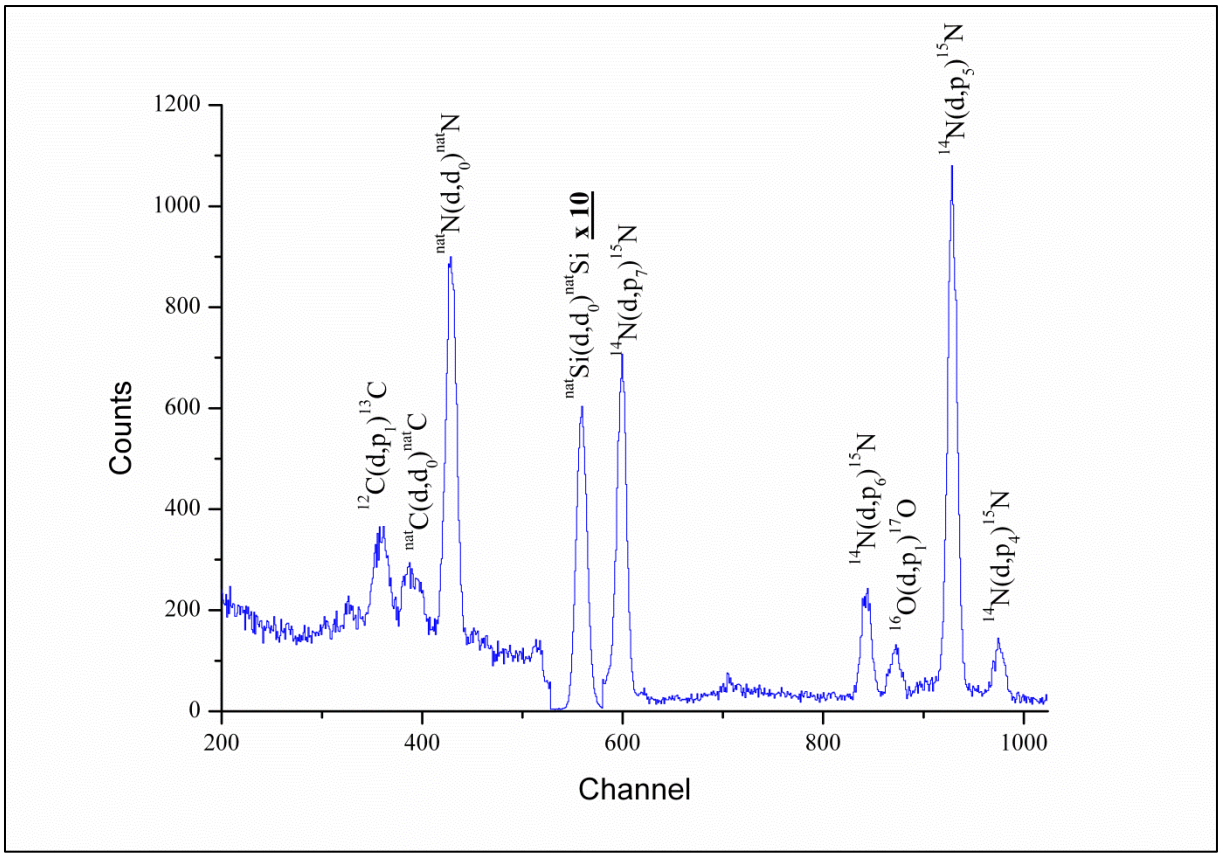
Counts
Channel
0
200
400
600
800
1000
1200
200
400
600
800
1000
$^{12}C(d,p_1)^{13}C$
$^{nat}C(d,d_0)^{nat}C$
$^{nat}N(d,d_0)^{nat}N$
$^{nat}Si(d,d_0)^{nat}Si$ x 10
$^{14}N(d,p_7)^{15}N$
$^{14}N(d,p_6)^{15}N$
$^{16}O(d,p_1)^{17}O$
$^{14}N(d,p_5)^{15}N$
$^{14}N(d,p_4)^{15}N$

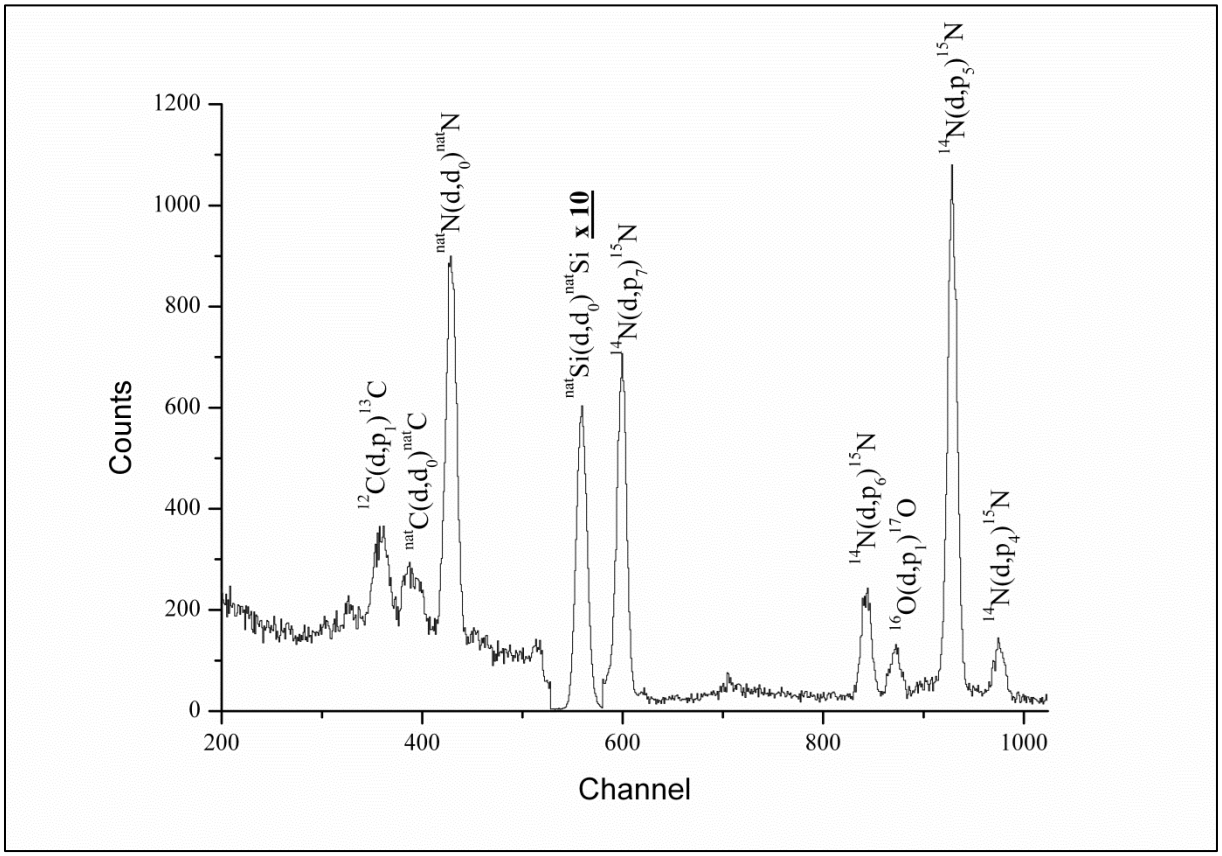
Counts
Channel
0
200
400
600
800
1000
1200
200
400
600
800
1000
$^{12}C(d,p_1)^{13}C$
$^{nat}C(d,d_0)^{nat}C$
$^{nat}N(d,d_0)^{nat}N$
$^{nat}Si(d,d_0)^{nat}Si$ x 10
$^{14}N(d,p_7)^{15}N$
$^{14}N(d,p_6)^{15}N$
$^{16}O(d,p_1)^{17}O$
$^{14}N(d,p_5)^{15}N$
$^{14}N(d,p_4)^{15}N$

Table 1.

Reactions	Energy of gamma rays (keV)	Initial state	Energy of the excited state (keV)	$A_2 \pm \Delta A_2$
$^{14}N(d,p\gamma_{4\text{-}1})^{15}N$	1885	5/2+	7155	0.085±0.014
$^{14}N(d,p\gamma_{6\text{-}1})^{15}N$	2297	7/2+	7567	-0.085±0.020
$^{14}N(d,p\gamma_{5\text{-}0})^{15}N$	7299	3/2+	7301	-0.015±0.014
$^{14}N(d,p\gamma_{7\text{-}0})^{15}N$	8310	1/2+	8312	0.038±0.030
$^{28}Si(d,p\gamma_{1\text{-}0})^{29}Si$	1273	3/2+	1273	-0.015±0.017
$^{28}Si(d,p\gamma_{2\text{-}0})^{29}Si$	2028	5/2+	2028	0.072±0.072
$^{28}Si(d,p\gamma_{3\text{-}0})^{29}Si$	2426	3/2+	2426	-0.230±0.026
$^{28}Si(d,p\gamma_{10\text{-}0})^{29}Si$	4934	3/2-	4934	-0.174±0.026

Fig. 3.

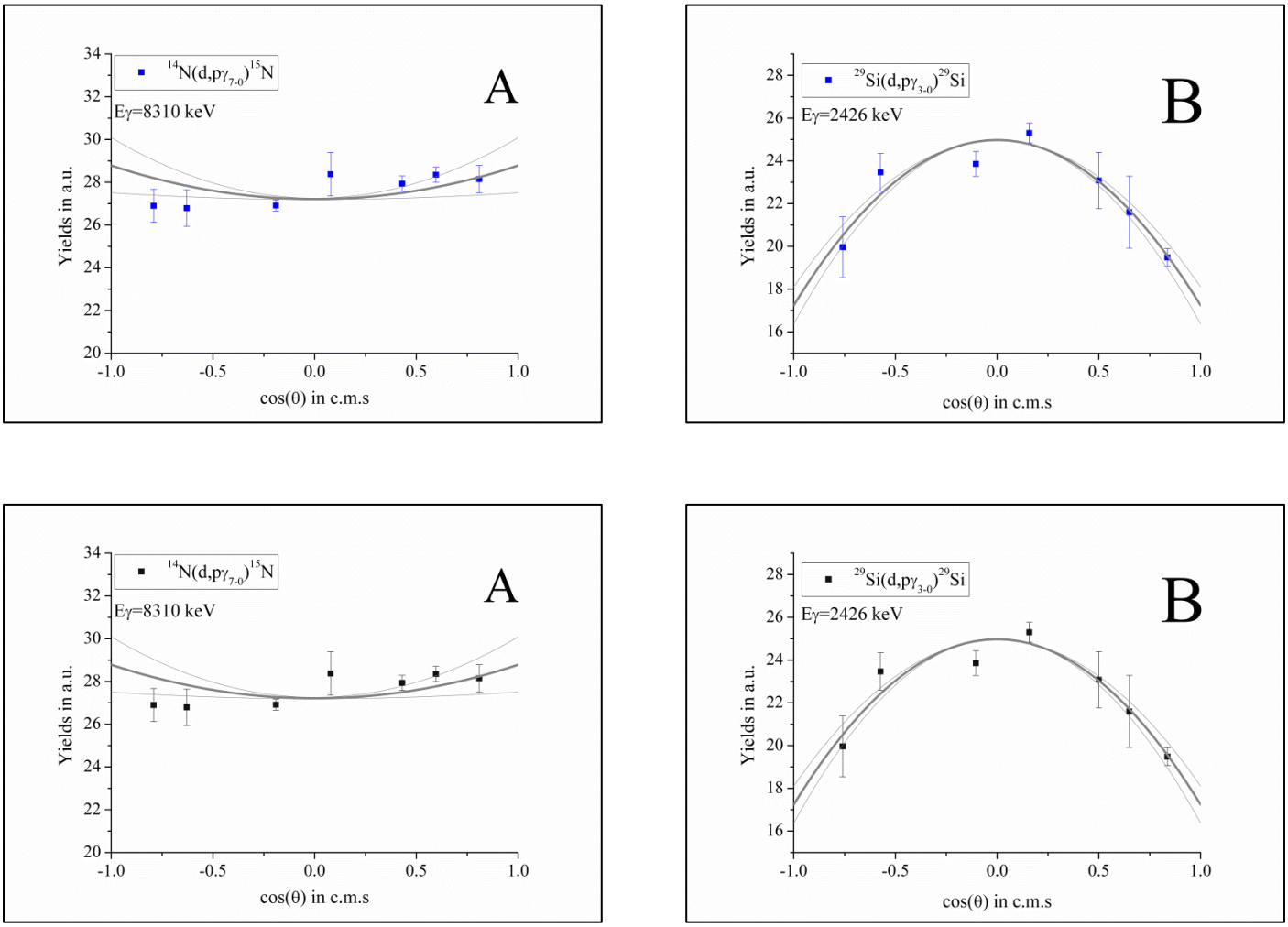

Fig. 4.

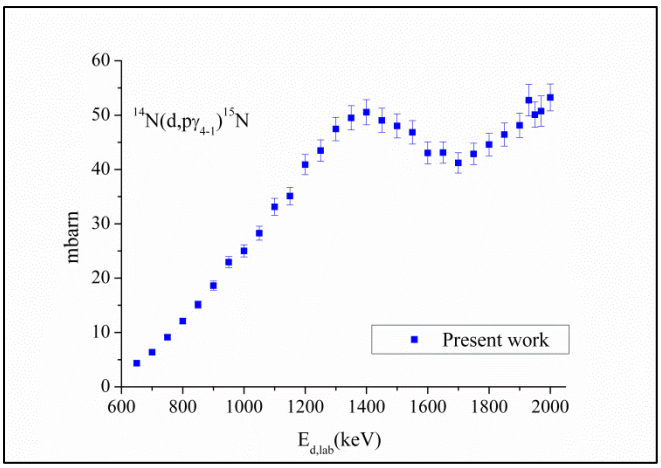
^{14}N(d,pγ_{4-1})^{15}N
mbarn
E$_{d,lab}$(keV)
Present work

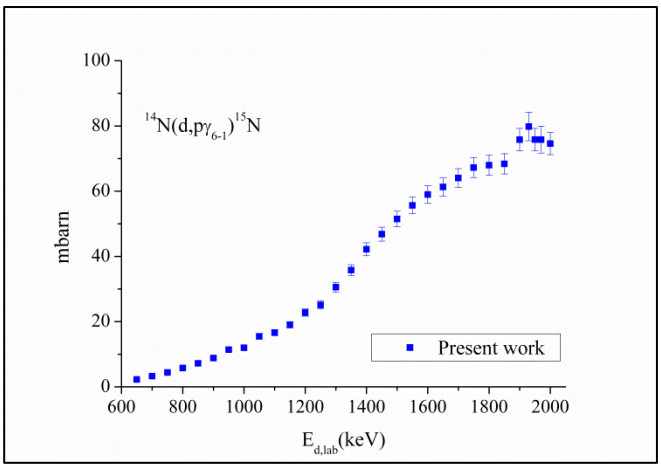
^{14}N(d,pγ_{6-1})^{15}N
mbarn
E$_{d,lab}$(keV)
Present work

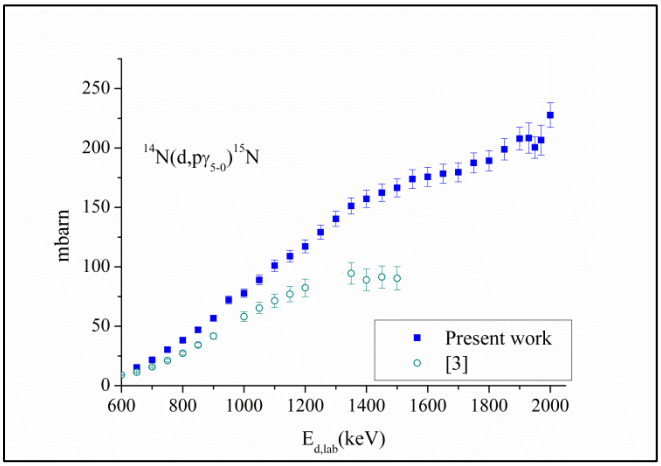
^{14}N(d,pγ_{5-0})^{15}N
mbarn
E$_{d,lab}$(keV)
Present work
[3]

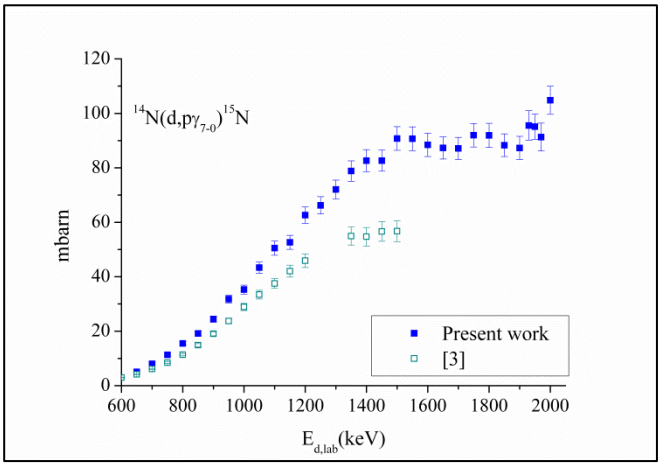
^{14}N(d,pγ_{7-0})^{15}N
mbarn
E$_{d,lab}$(keV)
Present work
[3]

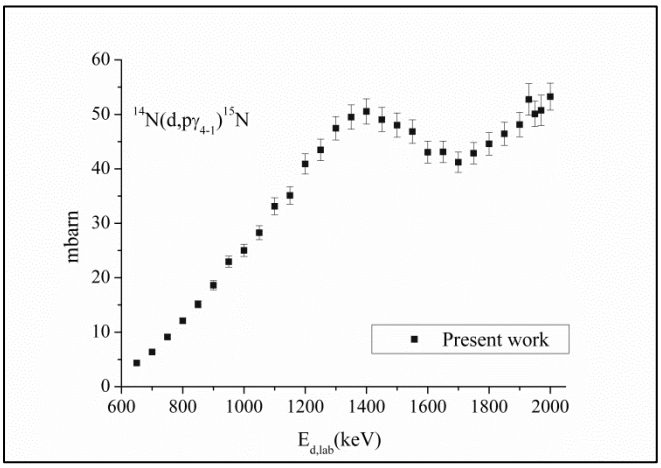
^{14}N(d,pγ_{4-1})^{15}N
mbarn
E$_{d,lab}$(keV)
Present work

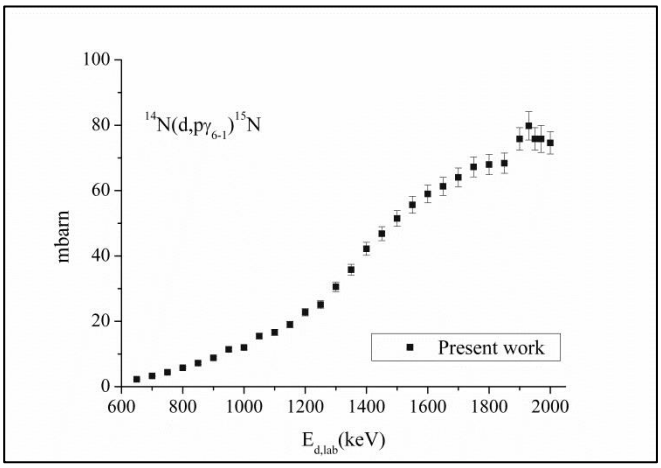
^{14}N(d,pγ_{6-1})^{15}N
mbarn
E$_{d,lab}$(keV)
Present work

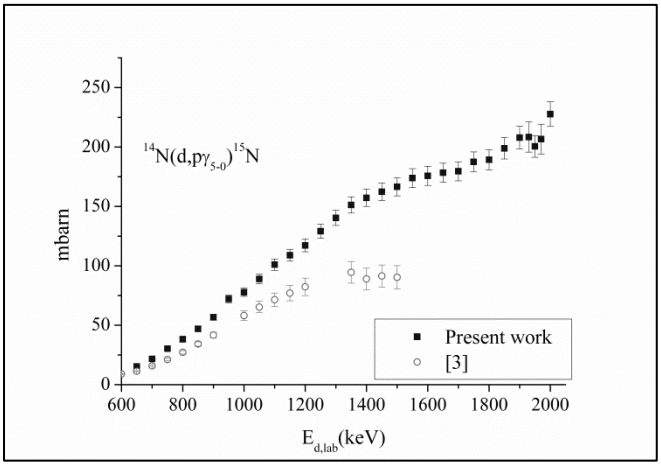
^{14}N(d,pγ_{5-0})^{15}N
mbarn
E$_{d,lab}$(keV)
Present work
[3]

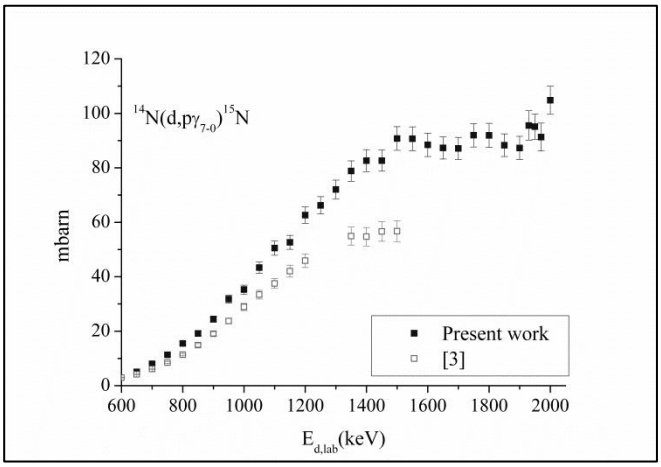
^{14}N(d,pγ_{7-0})^{15}N
mbarn
E$_{d,lab}$(keV)
Present work
[3]

Fig. 5.

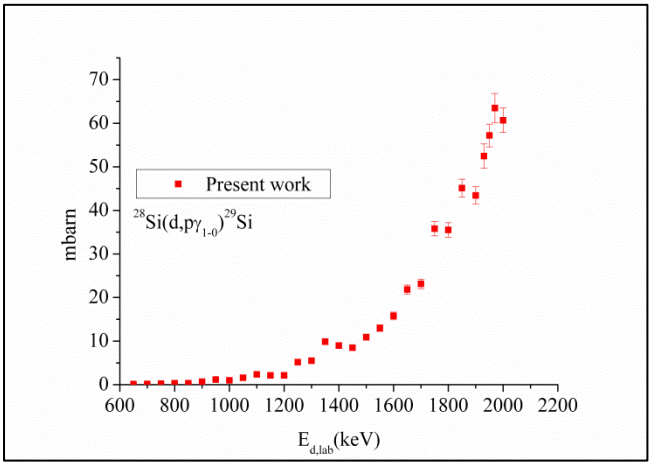
Present work
^{28}Si(d,pγ$_{1-0}$)^{29}Si
mbarm
E$_{d,lab}$(keV)

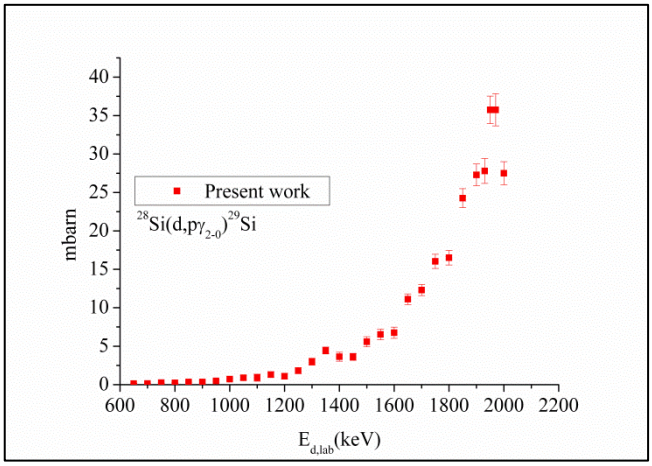
Present work
^{28}Si(d,pγ$_{2-0}$)^{29}Si
mbarm
E$_{d,lab}$(keV)

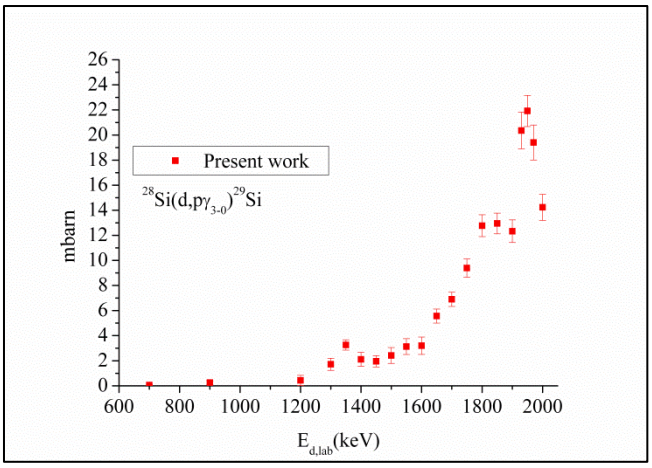
Present work
^{28}Si(d,pγ_{3-0})^{29}Si
mbarn
E$_{d,lab}$(keV)

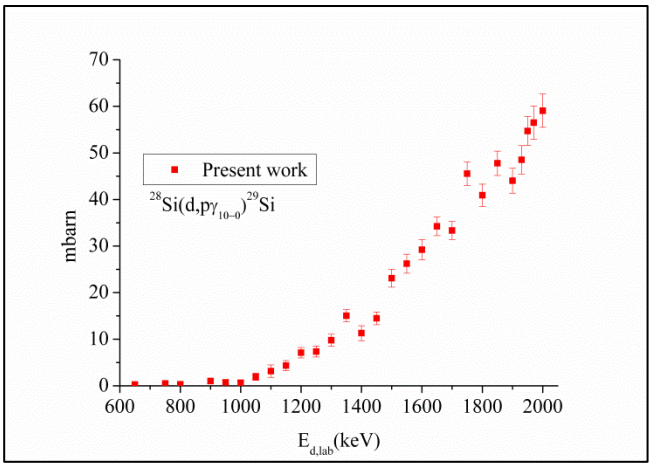
Present work
^{28}Si(d,pγ_{10-0})^{29}Si
mbarn
E$_{d,lab}$(keV)

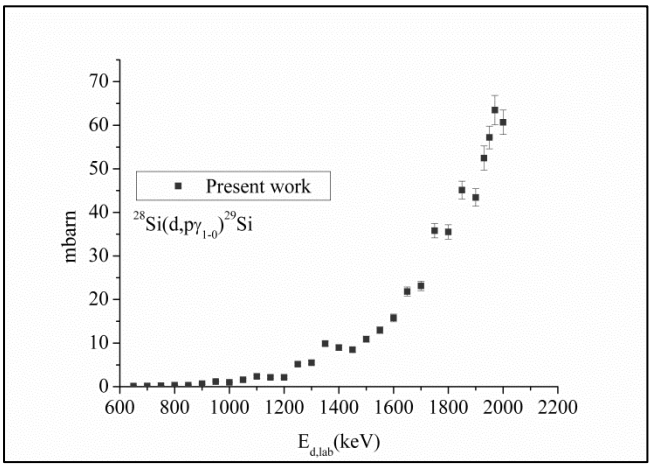
Present work
^{28}Si(d,pγ_{1-0})^{29}Si
mbarn
E$_{d,lab}$(keV)

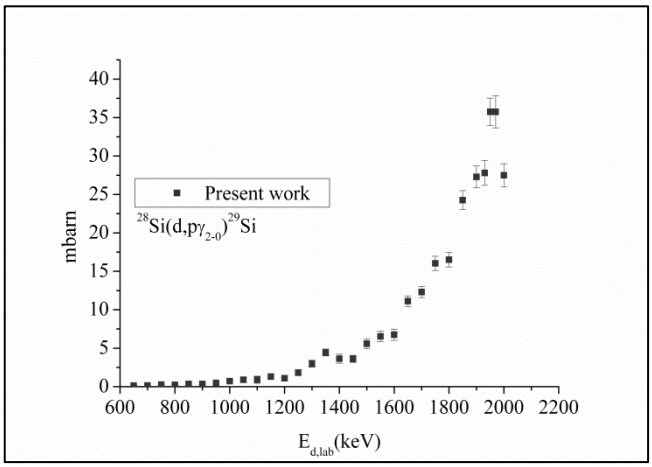
Present work
^{28}Si(d,pγ_{2-0})^{29}Si
mbarn
E$_{d,lab}$(keV)

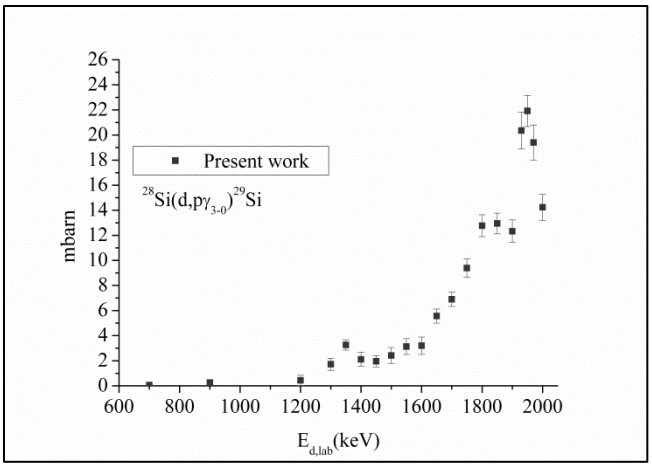
Present work
^{28}Si(d,pγ_{3-0})^{29}Si
mbarn
E$_{d,lab}$(keV)

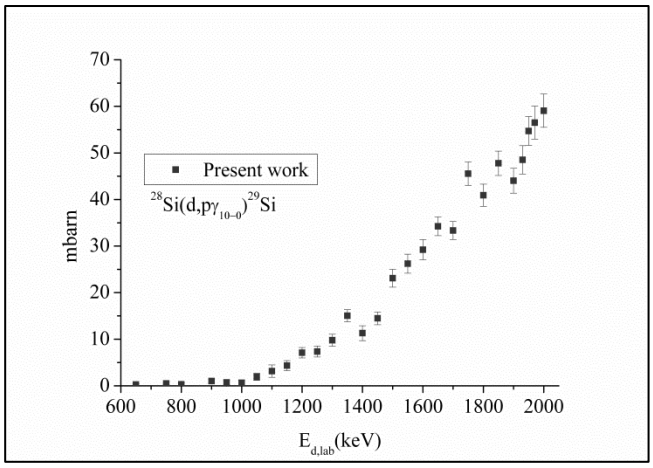
Present work
^{28}Si(d,pγ_{10-0})^{29}Si
mbarn
E$_{d,lab}$(keV)

Fig. 6.

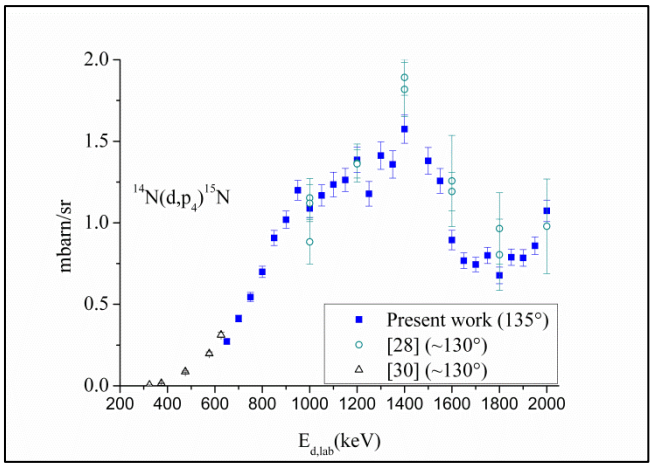
^{14}N(d,p$_4$)^{15}N
Present work (135°)
[28] (~130°)
[30] (~130°)
mbarn/sr
E$_{d,lab}$(keV)

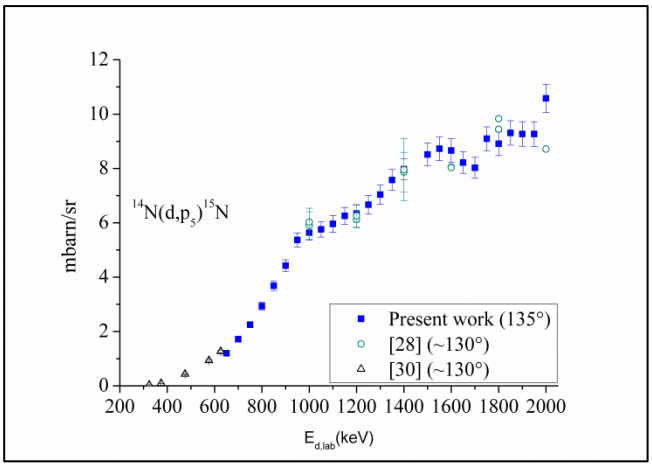
^{14}N(d,p$_5$)^{15}N
Present work (135°)
[28] (~130°)
[30] (~130°)
mbarn/sr
E$_{d,lab}$(keV)

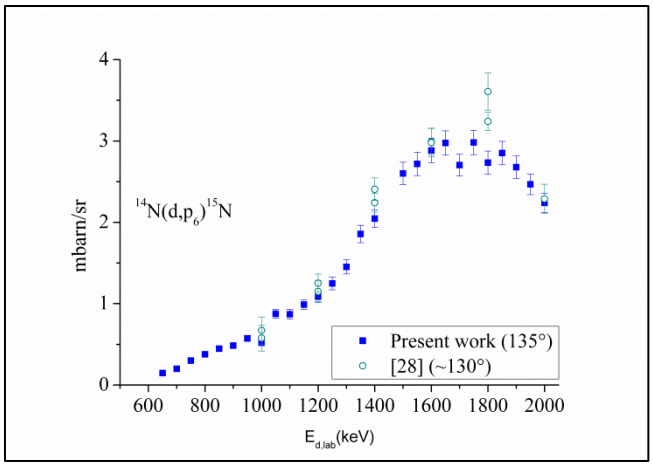
mbarn/sr
^{14}N(d,p$_6$)^{15}N
Present work (135°)
[28] (~130°)
E$_{d,lab}$(keV)

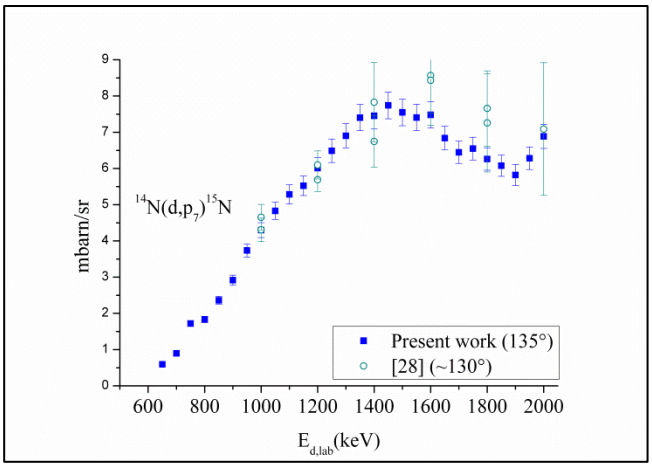
mbarn/sr
^{14}N(d,p$_7$)^{15}N
Present work (135°)
[28] (~130°)
E$_{d,lab}$(keV)

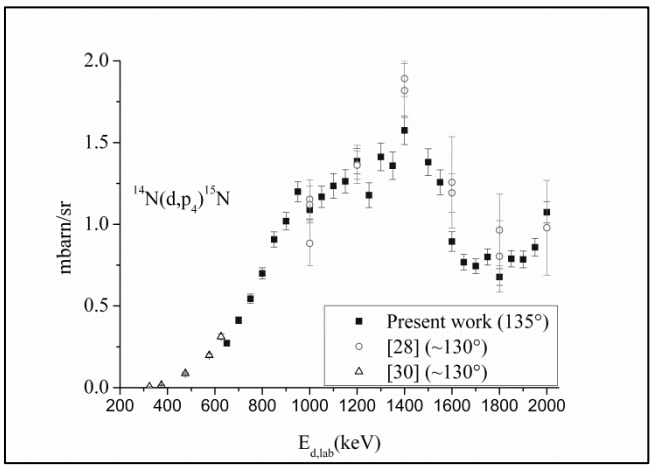
mbarn/sr
^{14}N(d,p$_4$)^{15}N
Present work (135°)
[28] (~130°)
[30] (~130°)
E$_{d,lab}$(keV)

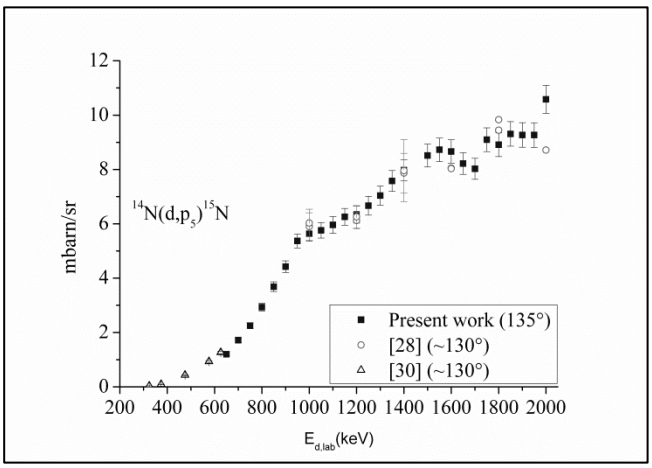
mbarn/sr
^{14}N(d,p$_5$)^{15}N
Present work (135°)
[28] (~130°)
[30] (~130°)
E$_{d,lab}$(keV)

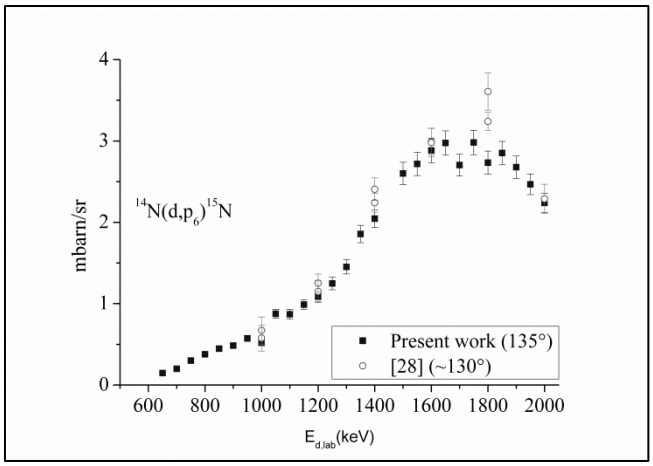
^{14}N(d,p$_6$)^{15}N
mbarn/sr
E$_{d,lab}$(keV)
Present work (135°)
[28] (~130°)

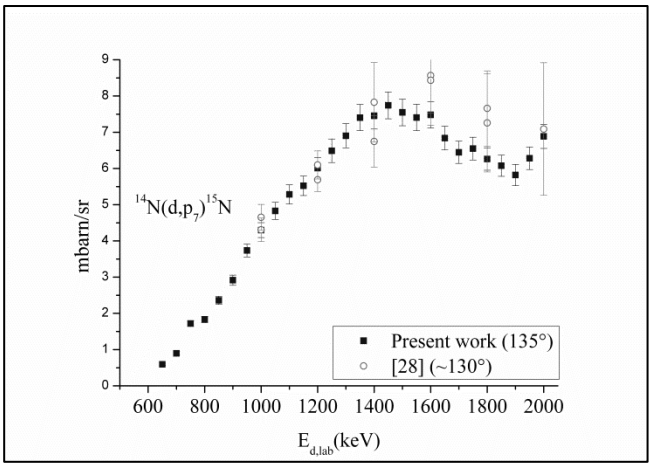
^{14}N(d,p$_7$)^{15}N
mbarn/sr
E$_{d,lab}$(keV)
Present work (135°)
[28] (~130°)

Fig. 7.

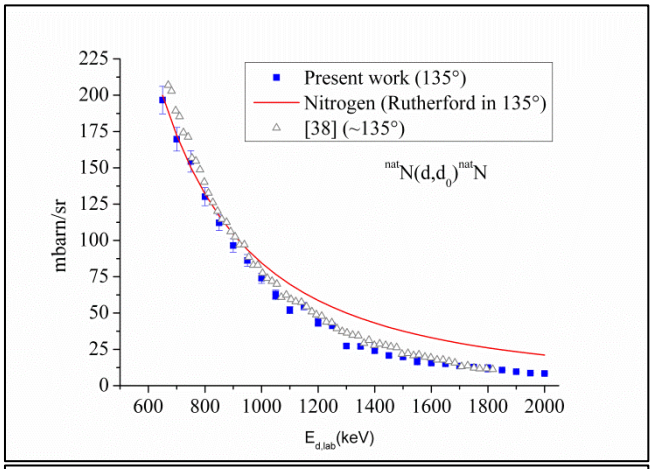
^{nat}N(d,d$_0$)^{nat}N
mbarn/sr
E$_{d,lab}$(keV)
Present work (135°)
Nitrogen (Rutherford in 135°)
[38] (~135°)

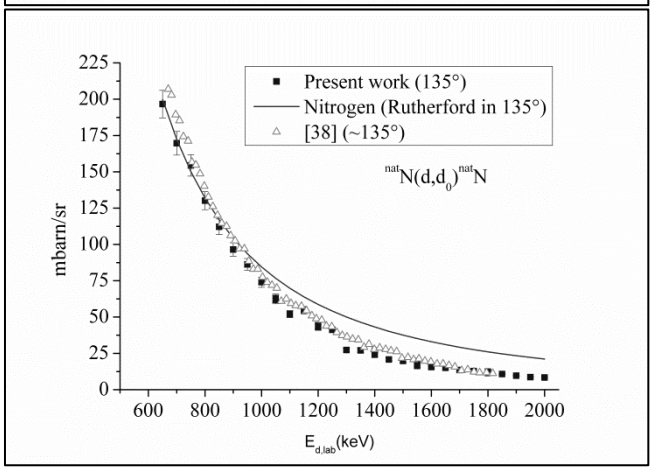
^{nat}N(d,d$_0$)^{nat}N
mbarn/sr
E$_{d,lab}$(keV)
Present work (135°)
Nitrogen (Rutherford in 135°)
[38] (~135°)